Volume 1 | Number 1 | Jan 2013 | Pages 1–100

Journal of
Materials Chemistry A

Materials for energy and sustainability
www.rsc.org/materialsA

ROYAL SOCIETY
OF CHEMISTRY

ROYAL SOCIETY
OF CHEMISTRY

www.rsc.org/materialsA

Journal Name

ARTICLE

Inorganic P-type contact materials for perovskite-based solar cells

Ming-Hsien Li,[a] Po-Shen Shen[a], Kuo-Chin Wang[a], Tzung-Fang Guo[a,b,c] and Peter Chen*[a,b,c]

Organic-inorganic hybrid perovskite solar cells are promising low-cost emerging photovoltaic devices due to their rapid progresses in conversion efficiencies. In this perspective, we review recent published works of perovskite-based solar cells incorporated with inorganic p-type hole transport layer. The current state-of-the-art devices of nickel oxide-based perovskite solar cells display a remarkably power of efficiency over 15%. In addition, solar cells using perovskite as light absorber and hole transporter without p-type contact material are also reviewed.

1. Introduction

With rapid progress being made in solid-state organometal lead halide perovskite, such as $CH_3NH_3PbX_3$ (X = I, Br, Cl), this material has attracted much attention because of its direct optical bandgap of around 1.5 eV,[1] low exciton binding energy,[2] long diffusion length,[3, 4] long carrier lifetimes, and broad absorption range from visible to near-infrared spectrum (800 nm) with high extinction coefficient ($\sim 10^{-4}$ cm^{-1} at 550 nm). Hence, perovskite is extensively utilized as a promising light absorber in low-cost photovoltaics. $CH_3NH_3PbI_3$ and $CH_3NH_3PbI_{3-x}Br_x$ were first employed to fabricate sensitized-type solar cells with iodide liquid electrolyte by Miyasaka's group,[5] and a power conversion efficiency (PCE) beyond 6% was further demonstrated by Park's group.[6] However, the perovskite materials are not stable in highly polar liquid electrolyte. A remarkable success for perovskite-based solar cell (PSC) was obtained by replacing the liquid hole-transporting medium into solid-state organic molecules or polymers as hole transport materials (HTM). The first realized solid-state perovskite-based solar cells using HTM of Spiro-OMeTAD (2,2',7,7'-tetrakis-(N,N-di-p-methoxyphenylamine)-9,9'-bifluorene) were fabricated with mesoscopic TiO_2 having a PCE exceeding 9% and with super-mesostructure Al_2O_3 scaffold over 10 %.[1, 7] Perovskite solar cells using Spiro-OMeTAD were continuously improved with optimization on the deposition methods of perovskite absorbers and interface control which delivered efficiency over 19%.[8]

The configurations of perovskite solar cells evolved from mesoscopic sensitized junction, non-injecting super-mesostructure Al_2O_3 scaffold, to thin film planar photovoltaic devices. Basically, the structure of organolead halides based hybrid solar cells can be categorized into mesoscopic junction (Figure 1(a) and 1(c)) or planar (Figure 1(b) and 1(d)) junction devices. For either mesoscopic or planar configuration, the devices can be constructed with n-i-p (Figure 1(a) and 1(b)) or p-i-n heterojunctions (Figure 1(c) and 1(d)) depending on which polarity of contact is applied as substrate layer. These four structures of PSC were illustrated in Figure 1. Perovskite solar cells based on mesoscopic layer which start with n-type contact substrate materials as n-i-p heterojunction photovoltaic were firstly investigated. Perovskite was employed as an intrinsic material (i) and light absorber. This structure mimics the conventional solid-state

dye-sensitized solar cells just by replacing the dye with peroskite, with the n-layer in general a wide band gap n-type oxide such as TiO_2 or ZnO. The p-type materials frequently used in this case are organic HTMs. Recently some inorganic materials like CuSCN,[9-12] CuI[13] and NiO[11, 14-22] have been demonstrated with success to work as p-type materials.
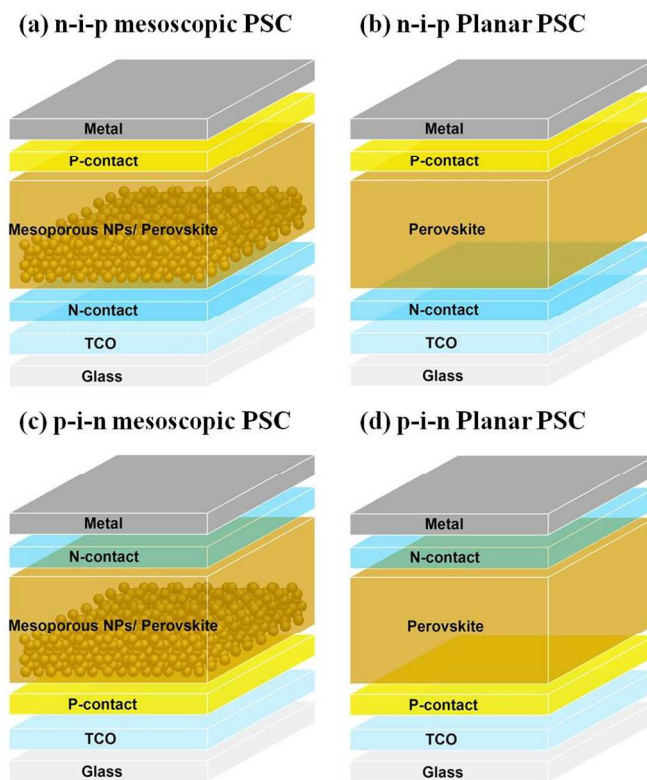
Figure 1. Device structures of (a) n-i-p mesoscopic, (b) n-i-p planar, (c) p-i-n mesoscopic and (d) p-i-n planar perovskite solar cells.

Briefly, a compact hole-blocking layer is first formed on top of the transparent conductive oxide (TCO) substrate, on which a pinhole-free and uniform layer is thus formed to suppress the recombination between carriers from the perovskite layers and TCO efficiently. On top of the compact layer, inorganic electron transport materials (ETM) accept the photo-excited electrons from the light absorber and transport them to the TCO anode. A mesoporous layer of n-type metal oxide semiconductor (such as TiO_2, ZnO) or scaffold (such as Al_2O_3, ZrO_2) is formed by spin-coating a nanoparticle paste, providing a highly porous matrix to adsorb perovskite. The perovskite films are subsequently deposited on top of the n-type mesoporous layer by spin-coating, two-step sequential deposition [23] or solvent engineering technique.[24, 25] The deposition of a HTM, such as organic hole conducting polymer of spiro-OMeTAD, with appropriate dopants to improve conductivity is utilized to extract and transfer holes from the valance band (VB) of the light absorber. Finally, a metal electrode is deposited on top of the HTM to complete the solar cell. Recently, the PCE was improved to achieve ~17% by using a two-step spin-coating procedure; involving spin-coating of PbI_2 film followed by spin-coating a solution of CH_3NH_3I to form cuboids $CH_3NH_3PbI_3$.[23]

With a feature of long diffusion length for perovskite, charge carrier diffusion lengths were observed to be more than 100 nm [3, 4] for $CH_3NH_3PbI_3$ and more than 1000 nm for $CH_3NH_3PbI_{3-x}Cl_x$ [4] based on a femtosecond transient optical spectroscopy study, including transient absorption and photoluminescence quenching measurements. As a result, planar heterojunciton (PHJ) device configurations are further proposed and attracting attention due to the removal of the mesoscopic layer, which simplifies device fabrication process with reduced material cost and sintering temperature. For planar structure, a uniform perovskite film is deposited by a variety of methods such as spin-coating, dual-source vapor deposition[26] and vapor-assisted solution processing.[27] By controlling the formation of the perovskite layer and careful choices of other materials, this planar structure has remarkably advanced the PCE close to 19% with n-i-p heterojunction. [8]

Although devices based on n-i-p heterojunction exhibit good performance, the diffusion length of hole is slightly shorter than that of electron due to a larger effective mass of hole.[3, 4] Therefore, mesoscopic (or planar) perovskite solar cells based on p-i-n heterojunction, which the substrate started with p-type selective contact, are recently studied [14-17, 28]. The perovskite films are deposited on the mesosopic (or compact) HTM layer. With the illumination from the p-side, the perovskite solar cell based on p-i-n heterojunction is feasible to have a charge generation profile with more effective hole extracton, as schematic presented in Figure 2. Furthermore, with holes flowing to the TCO substrate, it provides us more choices on the designs for integration of perovskite solar cells with silicon or copper indium gallium selenide (CIGS) solar cells to build tandem devices.
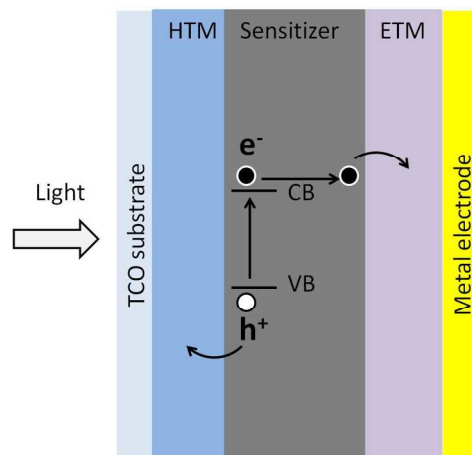
Figure 2. The scheme of carrier transport in the p-i-n heterojunction based on the perovskite sensitized solar cells.

Highly efficient perovskite solar cells have exclusively employed organic hole conducting polymers which are often expensive and have relatively low hole mobility. The stability is another concern for its long-term use. For example, PEDOT:PSS, the common organic hole extraction layer used in organic photovoltaic (OPV) is acidity and has tendency to absorb water. It is plausible on its use for the long-term stability. Hence, the use of organic hole conductors may cause a potential hurdle to the future commercialization of PSC from the consideration of cost and stability. Thus, providing more stable constituents of HTM for perovskite-based photovoltaics is required. In order to explore new inorganic hole conducting materials for these perovskite-based photovoltaics, inorganic p-type semiconductors are alternative hole transport materials due to their higher mobility, high transparency in the visible region, good chemical stability and various selections in terms of the VB energy level.

For the organic bulk heterojunction (BHJ) solar cells, p-type metal oxide semiconductors including NiO,[29, 30] V_2O_5,[31] MoO_3 [32, 33] have been utilized as hole extraction layer. In DSCs, many metal oxides such as NiO, Cu-based delafossite ($CuMO_2$, M = Al, Ga or Cr), have been applied as electrode for p-type sensitization. Recently, p-type sensitized NiO/perovskite heterojunction solar cells have been successfully demonstrated with decent efficiencies.[11, 14-22] The elimination of the organic hole transporter (or hole collecting layer) shall improve the device stability and provide versatile choices for materials selection and device design. Other inorganic materials such as CuI[13] and CuSCN[9-11] have been demonstrated to be potential candidate for this purpose. Copper iodide (CuI) was just reported as a hole conductor in perovskite-based mesoscopic n-i-p devices, showing a PCE of 6%. [13] Another interesting inorganic p-type semiconductor is copper thiocyanate (CuSCN), which shows good transparency throughout the visible and near infrared spectrum, high hole mobility of 0.01-0.1 $cm^2V^{-1}s^{-1}$ and good chemical stability.

In this review article, we focus on the recent developments in perovskite solar cells based on inorganic p-type semiconductor, including CuSCN, CuI and NiO. We first review the n-i-p heterojunction with planar or mesoscopic structure, followed by the review of p-i-n heterojunction. We would examine the recent studies on the carrier relaxation dynamics of perovskite/NiO heterojunction. Additionally, perovskite solar cells without HTMs are further discussed where the perovskite functioned as light absorber and hole

transporter. Lastly, we conclude the review with further possible improvements.

2. PSC based on inorganic HTM

(1). n-i-p heterojunction

In the n-i-p structure, we can simply replace organic HTM with inorganic p-type semiconductors. Copper-based inorganic semiconducting hole materials, such as CuSCN [34, 35] and CuI [36, 37], have shown promise for their use in dye-sensitized and quantum dot-sensitized solar cells. These materials can be deposited with solution process with good pore-filling. Meanwhile, these wide-band-gap semiconductors have high conductivity, suitable energy level and good transparency. It is intuitive to apply these materials with perovskite for photovoltaic application.

A. Mesoscopic PSC incorporated with CuSCN

An inorganic p-type semiconductor of copper thiocyanate (CuSCN), which shows good transparency throughout the visible and near infrared spectrum, high hole mobility and good chemical stability is firstly discussed. It can be deposited through doctor-blade process at low temperature, [9, 10] making it compatible with flexible substrates. Ito et al. first introduced CuSCN into mesoporous perovskite solar cell comprised of FTO/compact TiO_2/mesoporous TiO_2/$CH_3NH_3PbI_3$/CuSCN/Au. [10] In the fabrication process, the $CH_3NH_3PbI_3$ structure and thickness can be controlled by hot-air drying during spin coating, while CuSCN layer is deposited by using the doctor-blade process. With decreasing the $CH_3NH_3PbI_3$ thickness by hot-air drying and the addition of CuSCN layer, an improvement of the PCE was achieved from 1.35% to 4.85%. With the CuSCN hole conductor on $CH_3NH_3PbI_3$ film, the photocurrent considerably increased from 0.83 mA/cm^2 to 14.5 mA/cm^2. As a Sb_2S_3 layer is introduced at the interface between mesoporous TiO_2 and $CH_3NH_3PbI_3$, it enhanced the crystalline of perovskite structure and eliminated the PbI_2 formation. Therefore, PCE was improved to be 5.12% and the device presented stability against light exposure without encapsulation. [12] By further controlling the thickness of perovskite film (less than 1 μm), $CH_3NH_3PbI_3$ capping layer, and the optimized HTM layer of 600-700 nm, a promising PCE of 12.4% was achieved. [9] They demonstrated the same perovskite solar cell architecture consisting of TiO_2 as a scaffold as well as electron collector, perovskite as the light harvester and CuSCN as the HTM. With a compatible energy level as shown in Figure 3(a), the device displayed a promising performance with a short circuit current density of 19.7 mA/cm^2, an open-circuit voltage of 1,016 mV and a fill factor of 0.62, resulting in a PCE of 12.4%. As seen in Figure 3(b), with an effective charge extraction layer of CuSCN, the photovoltaic parameters have significant increased.
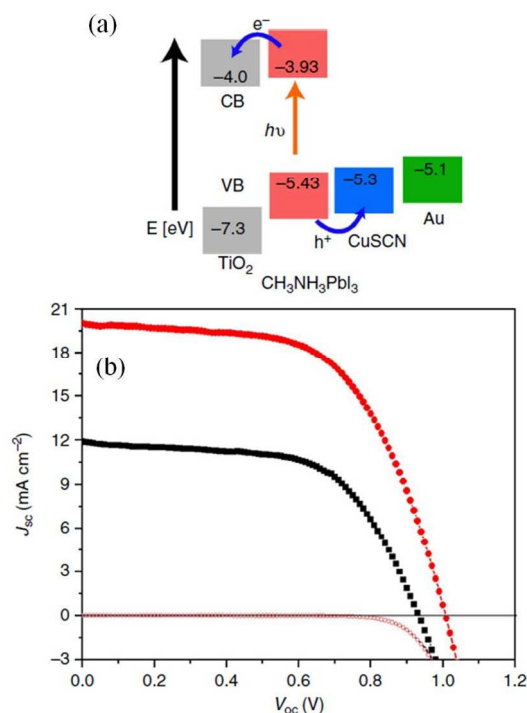
Figure 3. (a) Energy level diagram of the TiO_2/$CH_3NH_3PbI_3$/CuSCN/Au device with ideal electron injection and hole extraction. (b) J-V characteristics of the heterojunction solar cells with (red) and without (black) CuSCN. Reprinted with permission from ref. 9.

B. Mesoscopic PSC incorporated with CuI

Copper iodide (CuI) was selected on the basis of its suitable VB position, high p-type conductivity, and the compatibility of the solution deposition method with the perovskite absorber. Kamat et al. employed CuI as hole conducting materials, and a PCE of 6.0% with excellent photocurrent stability was achieved. [13] Device of solar cell was constructed as FTO/compact TiO_2/mesoscopic TiO_2/$CH_3NH_3PbI_3$/CuI/Au. In the fabrication process, the perovskite film was deposited by one-step spin-coating of CH_3NH_3I and PbI_2 in γ-butyrolactone and then annealed to complete crystallization. Solution deposition of CuI was performed by automated drop-casting technique. [34] The open-circuit voltage, compared to the best spiro-OMeTAD devices, remains low and is attributed to higher recombination in CuI devices as determined by impedance spectroscopy. However, impedance spectroscopy revealed that CuI exhibits 2 orders of magnitude higher electrical conductivity than spiro-OMeTAD which allows for significantly high fill factors of ~0.6. Reducing the recombination in these devices could render CuI as a cost-effective hole conductor in perovskite solar cells.

C. Mesoscopic PSC incorporated with NiO

For mesoscopic PSC based on NiO, Liu et al. employed mesoporous NiO as a spacer layer between the mesoporous TiO_2 and the carbon electrode. The perovskite solar cell is based on the structure composed of FTO/compact TiO_2/mesoporous TiO_2/sequential deposited $CH_3NH_3PbI_3$/mesoporous NiO/carbon. The energy landscape at the NiO/TiO_2 junction is a hetero p-n junction that separate electron and hole flow in different direction. Low recombination would occur at this interface. The mesoporous

NiO layer effectively adsorbed perovskite and facilitated the hole extraction, resulting in an impressive PCE of 11.4%.[38] This device can be fabricated under atmosphere condition due to the use of fully inorganic materials as the solar cell constituent.

(2). p-i-n heterojunction
A. Planar PSC incorporated with CuSCN

Sabbiah et al. reported the p-i-n type device architecture consisted of FTO/electrodeposited CuSCN/vapour-deposited $CH_3NH_3PbI_{3-x}Cl_x$/PCBM/Ag, which was fabricated under ambient condition, with a maximum PCE of 3.8%.[11] Photoluminescence (PL) quenching of the perovskite emission on CuSCN was performed as seen in Figure 4. A considerable decrease in PL intensity was observed as the perovskite film deposited on CuSCN with a excitation wavelength of 530 nm. Despite CuSCN showing effective quenching ability, higher series resistance (R_S) and shunt resistance (R_{SH}) may cause poor photovoltaic parameters of PSC with CuSCN.
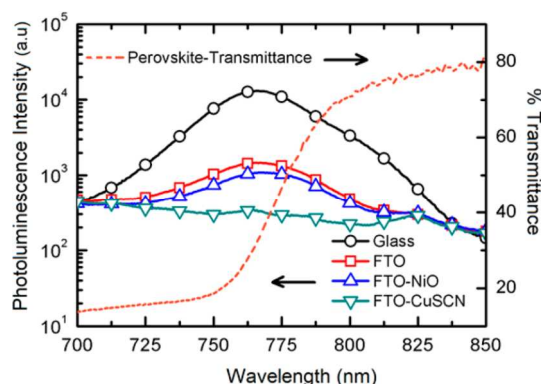
Figure 4. Photoluminescence of $CH_3NH_3PbI_{3-x}Cl_x$ coated on glass, FTO, FTO/NiO, and FTO/CuSCN. Reprinted with permission from ref. 11.

B. Planar PSC incorporated with NiO

Nickel oxide is a cubic p-type metal oxide material with a large band gap. It has been widely used as interfacial layer in OPV[29] or photocathode in conventional liquid junction p-type dye-sensitized solar cells (DSCs).[30, 39-41] Some p-type materials have been investigated in conjunction with perovskite film for PL response.[42] It was the first evidence that NiO was able to effectively quench the PL spectrum of perovskite although complete device combining NiO and perovskite was not fabricated due to poor perovskite film formation and poor surface coverage. For the fabrication of the first planar $NiO/CH_3NH_3PbI_3$ heterojunction solar cells, we applied a solution processed NiO_x thin film electrode interlayer on the glass/ITO electrode to realize the efficient $CH_3NH_3PbI_3$/PCBM PHJ hybrid solar cells.[15] As reported above, NiO_x as expected is a potential electrode interlayer for the charge transfer of hole from the PL spectrum. To resolve the coverage issue, a UV-Ozone treatment of glass/ITO/NiO_x substrate was performed to modify the work function to improve the photovoltaic parameters and surface wetting properties to improve surface coverage, as seen in the ultraviolet photoelectron spectrum (UPS) shown in Figure 5. The work function of NiO_x electrode interlayer is estimated to be 5.4 eV with a reduced water contact angle that significantly improves the surface coverage of perovskite film.
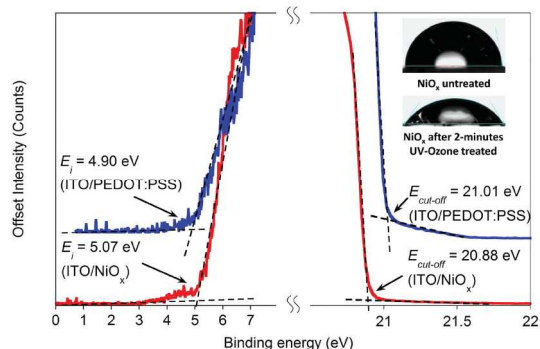
Figure 5. UPS of the surface measurement for UV-ozone treated glass/ITO/NiO_x substrates. Insets: Photographs of the water contact angle for the untreated and treated glass/ITO/NiOx substrate. Reprinted with permission from ref. 15.

The hybrid cell of glass/ITO/spin-coated NiO_x/one-step deposited $CH_3NH_3PbI_3$/PCBM/BCP/Al was produced with a PCE of 7.8%. Sabbiah et al. also reported the similar architecture of FTO/electrodeposited NiO/vapour-deposited $CH_3NH_3PbI_{3-x}Cl_x$/PCBM/Ag with the replacement of CuSCN by NiO.[11] Since R_S and R_{SH} for PSC with NiO film are about lower than an order of magnitude, a higher PCE of 7.3% was obtained. Hu et al. presented the same device architecture of ITO/spin-coated NiO/sequential deposited $CH_3NH_3PbI_3$/PCBM/Al with a UV-ozone treatment to achieve a device PCE of 7.6%.[14] However, in lack of a hole blocking layer of BCP, the obtained PCE was slightly lower than that reported by Chen and Guo groups.[15] With further improvement in the quality of NiO film, Cui et al. exploited reactive magnetron sputtering method to prepare compact NiO film.[19] A planar PSC was constructed as FTO/sputtered NiO/solvent-engineering $CH_3NH_3PbI_3$/PCBM/BCP/Au. The solvent-engineering method had benefit to form a homogeneous surface coverage and uniform interlayer morphology; hence PCE was promoted to achieve 9.84%.[19] Furthermore, significant improvements were advanced in mesoscopic NiO film to increase light harvest or by doping in NiO film. Cu was employed as a dopant in NiO_x film to modulate conductivity. The device configuration proposed by Kim et al. is ITO/Cu-doped NiO_x/solvent engineering $CH_3NH_3PbI_3$/$PC_{61}BM$/C_{60}/Ag. PCE of planar PSC based on Cu-doped NiO_x film can be significantly improved to be 15.4%, which was attributed to the improved electrical conductivity and favourable perovskite crystallization.[20] The highly doped NiO has a higher work function that match well with the wider bandgap perovskite materials using other halide such as Br. The favourable energy level matching between the work function of Cu-doped NiO and the VB of Br-containing $(MAPb(I_{0.6}Br_{0.4})_3)$ perovskite allowed high voltage output of 1.16 V.

C. Mesoscopic PSC incorporated with NiO

For the fabrication of mesoscopic $CH_3NH_3PbI_3$ heterojunction solar cells, two results were reported nearly at the same time. Tian et al. reported PSC based on mesoporous NiO film. A architecture of FTO/compact NiO/mesoporous NiO/$CH_3NH_3PbI_3$/PCBM/Al was fabricated.[18] By controlling the thickness of compact NiO layer of 80 nm with mesoporous NiO film of 120 nm, the best PCE of 1.5% was obtained. However, the IPCE spectra of the $CH_3NH_3PbI_3$ deposited on mesoporous NiO film was extremely low, the response of

$CH_3NH_3PbI_3$ was far from optimal with low PCE of 0.31% and J_{SC} of 1.45 mA/cm^2 obtained.

Another similar device reported by our group incorporated a mesoporous NiO layer into the planar device to adsorb more amount of perovskite, resulted in a significant improvement of the photovoltaic performance.[17] The full device structure of ITO/compact-NiO/spin-coated mesoporous NiO/sequential deposited $CH_3NH_3PbI_3$/$PC_{61}BM$/BCP/Al is shown in Figure 6(a) with the energy level of each material illustrated in Figure 6(b). This arrangement is appropriate for receiving high voltage with minimum loss providing the charge separation process between the absorber and selective contacts. The best-performing cell using $PC_{61}BM$ delivered high V_{OC} of 1040 mV with J_{SC} of 13.24 mA/cm^2 and 69% fill factor, leading to an overall PCE of 9.51%. The high V_{OC} received from the junction demonstrated the advantage of energy level alignment between light absorber and the contact materials. The energy loss in charge extraction is minimized by using $PC_{61}BM$ whose LUMO is nearly identical with the conduction band (CB) edge of perovskite while the mesoporous- NiO's VB edge is close to the VB of perovskite. The implement of mesoscopic NiO layer obviously improved photovoltaic performances for increased current response at the long wavelength part and voltage with respect to the PHJ cell.[15]
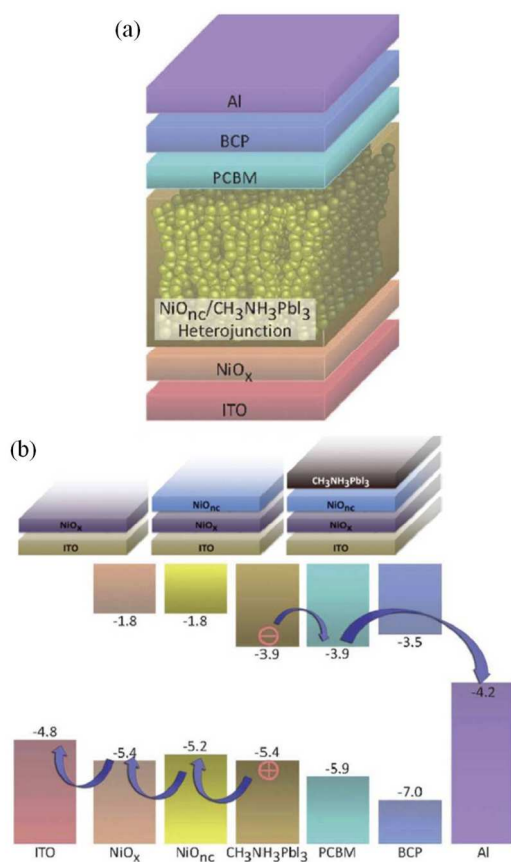
Figure 6. (a) The schematic of the solar cell device. (b) The energy level diagram of the mesoscopic NiO_{nc}/perovskite/PCBM heterojunction. Reprinted with permission from ref. 17.

From the IPCE and calculated light harvesting efficiency (LHE) in Figure 7, the mesoscopic NiO film seemed to be thick enough to absorb 90% of the incident light. However, the IPCE of the device seem to be lower than the state-of-the-art devices. There still exists some charge collection losses in the NiO/perovskite mesoscopic junction. Further improvements on the material quality of compact NiO film with better crystallinity shall be beneficial. Smaller particle size and well-dispersed mesoporous nanostructure are expected to promote the overall photovoltaic performance of this p-type oxide/perovskite heterojunciton.
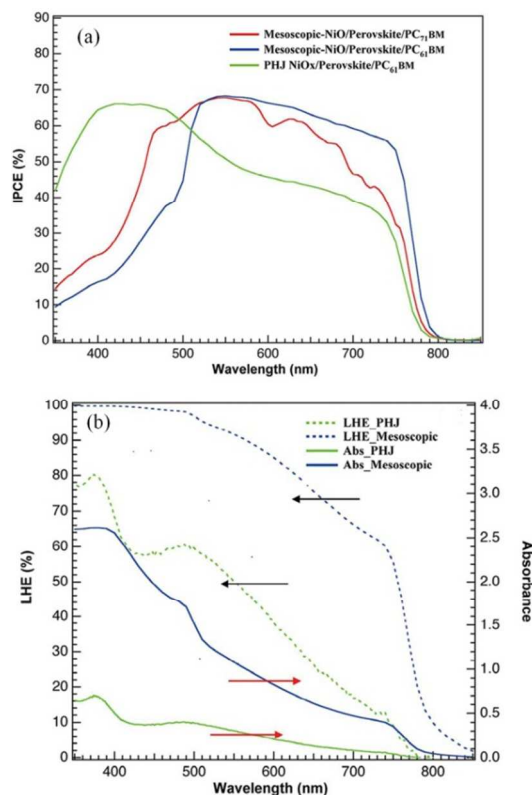
Figure 7. (a) The IPCE and (b) LHE of mesoscopic NiO/perovskite/$PC_{61}BM$ device heterojunction solar cell. Reprinted with permission from ref. 17.

Zhu et al. also reported similar work employing a mesoporous NiO film as hole extraction and transport layer for perovskite solar cell without compact NiO layer.[21] Appropriate controlled aggregation of the faceted NiO nanocrystals resulted in a corrugated surface that could support perovskite crystals with good coverage and interconnectivity. By increasing thickness of mesoporous NiO film from 20 to 40 nm, the electron blocking ability was improved; the charge recombination and leakage current were reduced. However, for the film-thickness increase from 40 to 70 nm, the decrease in photocurrent and voltage was most likely due to the increased series resistance and absorption of the mesoporous NiO film. With optimized thickness of mesoporous NiO layer of 40 nm, the best performance of the perovskite solar cell cell exhibited PCE of 9.11%, J_{SC} of 16.27 mA/cm^2 and V_{OC} of 882 mV.

In the following progress, we introduced low-temperature sputtered NiO_x film to form a pinhole less compact layer to prevent the charge collection losses causing by the solution-processed

compact NiO layer. The efficiencies are greatly enhanced and the device reproducibility is significantly improved compared with the devices fabricated by solution-processed NiO_x thin film.[17] Similar device architecture of ITO/sputtered NiO_x/mesoporous NiO/sequential-deposited $CH_3NH_3PbI_3$/PCBM/BCP/Al was demonstrated by deposition of compact NiO_x film with an RF magnetron sputtering system in pure Ar or reactive sputter method under a mixture of Ar and O_2 gas. With optimized doping oxygen flow ratio of 10% and thickness of mesoporous NiO layer, a PCE of 11.6% was obtained.[16] Compared with the p-i-n heterojunctions PSC based on PEDOT:PSS, a much higher PCE of 14.1% was achieved with the configuration of ITO/PEDOT/$CH_3NH_3PbI_3$/PCBM/LiF/Al.[28] It indicated that PSCs based on NiO still have much room to improve their performance. In order to minimize the light harvesting and interfacial recombination loss, Chen et al. utilized the super-mesostructure Al_2O_3 scaffold to replace the mesoporous NiO layer to fabricate the device architecture of ITO/spray NiO_x/mesoporous Al_2O_3/solvent engineering $CH_3NH_3PbI_3$/PCBM/BCP/Ag. Synchronized improvements in V_{OC}, J_{SC}, FF lead to a remarkable PCE of 13.5%.[22]

3. Charge separation and relaxation dynamics of perovskite/NiO junction

Although several reports have demonstrated PL quenching effect of perovskite/NiO junction, direct evidence of charge separation need to be examined. The PL spectra of perovskite coated on Al_2O_3 or NiO with similar intensity of UV/Vis absorption are shown in Figure 8. It is noted that a large band gap material of Al_2O_3 does not quench the PL and could be considered as a scaffold layer. To quantitatively analyze the PL quenching of both films, as seen in the UV/Vis absorption, the steady-state PL spectra with excitation at 450 nm were recorded (dashed curves in Figure 8) due to their similar absorption. The PL intensity of the perovskite coated on the NiO film was quenched more significantly than that of perovskite deposited on the Al_2O_3 film. The PL quenching of perovskite excitons might be caused by the extraction of the charge carriers across the interface through a p-type hole-extraction layer or charge recombination in the defects of perovskite layer. To explore the charge separation, we performed the photoinduced absorption (PIA) experiment to show that effective charge separation occurred at the NiO/perovskite interface.[17] In Figure 9, it is obvious that free carrier absorption is presented at the junction between NiO/perovskite. On the other hand, when perovskite in contact with non-injecting wide band gap materials (Al_2O_3 and glass), no such IR transient absorption feature is present.

For the carrier relaxation, Diau group demonstrated the dynamics of carrier relaxation in two device configurations of mesoporous NiO/perovksite and mesoporous Al_2O_3/perovksite employing femtosecond photoluminescence up-conversion spectroscopy.[43]
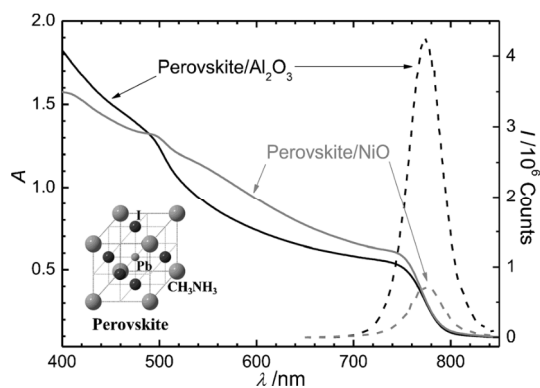
Figure 8. Absorbance (solid line) and photoluminescence (dash line) spectra of perovskite/Al_2O_3 (black) and perovskite/NiO (gray) films. Reprinted with permission from ref. 43.
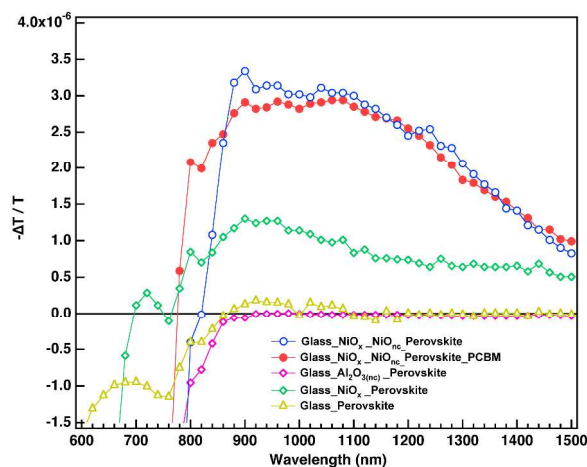
Figure 9. The photoinduced absorption (PIA) spectra of perovskite in contact with various materials. Reprinted with permission from ref. 17.

The relaxation mechanism is presented in Figure 10. The excitation at 450 nm invokes a transition from the VB2 state to the hot CB state; the probe at 670 and 770 nm correspond to the transitions of hot CB→VB1 and cold CB→VB1, respectively. The transient followed the kinetic model containing two sequential relaxations in parallel: (R1) A→B→C and (R2) A→B'→C'. Component A represents hot electrons relaxation of $CH_3NH_3PbI_3$ in the CB state. The carriers thermalized to CB edge subsequently produce components B and B', respectively. Components B and B' represent the relaxation to the surface state (SS; C) and the internal recombination relaxation to the VB1 state (C'), respectively. In experimental measurement, the temporal emission of PL transients were probed in the spectral region 670-810 nm, in which individual PL transient was deconvoluted into one rapid-decay (0.2~0.5 ps) of component A (contribution from hot carrier relaxation) and two slow-decay of components B (20 ps ~50 ps for surface state relaxation), and B' (0.5 ~1.2 ns for recombination). The rate of the decay of component B are similar for both films, while the values of

the decay coefficient of component B' (τ_3^{-1}) of the Al$_2$O$_3$ film are significantly greater than those of the NiO film. The similar relaxation times of τ_2 observed for both Al$_2$O$_3$ and NiO films implied that it is the intrinsic relaxation process occurred on the surface of the perovskite. For the amplitude for component B, the intensity in NiO/perovskite film is greater than that of Al$_2$O$_3$/perovksite which indicated the quenching by non-emissive surface state is more prevailing. The observed quenching of the steady-state PL intensity of perovskite shown in Figure 9 might be attributed to the surface-state relaxation of perovskite, which is more significant for the NiO film than for the Al$_2$O$_3$ film. The hole extraction time from perovskite by the NiO is estimated to be around 5 ns at the PL maximum of 770 nm.
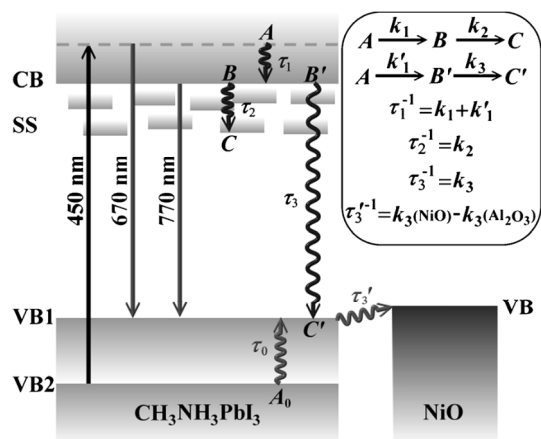
Figure 10. Mechanism of excitonic relaxation showing radiative and non-radiative processes observed for perovskite coated on mesoporous NiO semiconductor films. A kinetic model for fitting the PL transients is shown on the top right box. Reprinted with permission from ref. 43.

4. Perovskite as HTMs

Except for the standard perovskite/TiO$_2$ heterojunction solar cells employing organic/inorganic HTMs, the concept of hole-conductor-free perovskite heterojunction solar cells also attracts attentions as alternatives to the low-cost photovoltaic devices. The first mesoscopic PSC without HTM is successfully demonstrated by Etgar et al. with a PCE of 5.5%, and the perovskite simultaneously served as light harvester and hole conductor.[44] With advanced deposition technology for perovskite formation, such as two-step sequential deposition method, the device efficiency was further enhanced beyond 10%.[45-48] Soon, the planar PSC without the presence of HTM delivered a PCE over 5% with inverted p-i-n heterojunction structure using the configuration of ITO/perovskite/C$_{60}$/Ag.[49] In general, thermal evaporation of noble metal (Au or Ag) is still the major option for the deposition of back electrodes. Nevertheless, this process is energy-consuming and high-cost. In order to further reduce the fabrication cost, the evaporation process is considered to be replaced or even eliminated. Utilizing the successful concept of porous carbon material as cathode in DSCs, carbon has demonstrated as a promising counter electrode candidate

due to its similar work function compared with Au (-5.1 eV). Therefore, carbon-based mesoporous electrode is adapted to fully printable laminated carbon/ZrO$_2$/TiO$_2$ PSCs without HTM and metal electrode, reaching an initial PCE of 6.64%.[50] After further effort on the deposition methods or film thickness control, the best device efficiency of HTM-free carbon-based mesoporous PSCs has boosted up to 12.8% so far.[51-54] This configuration eliminated most of the organic components in the perovskite solar cells and showed a good performance in stability.

Conclusions

In conclusion, we summarized the recently reported perovskite solar cell based on inorganic p-type materials with their champion photovoltaic parameters summarized in **Table 1** and Figure 11. The replacement of the organic hole transport materials by inorganic p-type HTM has the advantages to provide robust device architecture for further development of all-inorganic perovskite-based solar cells and tandem photovoltaics. With further improvement on the perovskite deposition methods such as solvent engineering technique achieving high efficiency on mesoscopic structure [25] and planar structure[24], higher efficiency are expected for inorganic p-type perovskite solar cells.
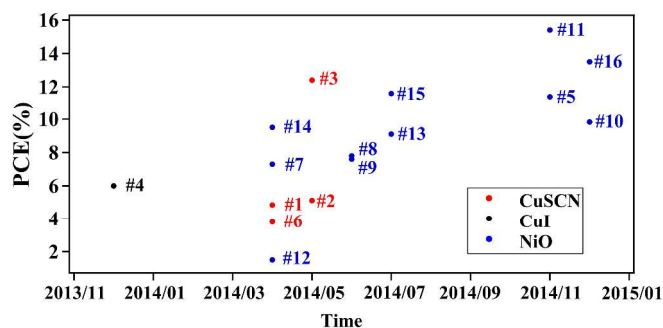
Figure 11. PCE revolution of PSC based on inorganic p-type semiconductor.

Journal Name

RSC**Publishing**

ARTICLE

Table 1. Summary of photovoltaic parameters of PSC based on inorganic p-type semiconductor.

number	Types	HTM	Device Structure	Photovoltaic Parameters			Ref.
				V_{OC} (mV)	J_{SC} (mA/cm^2)	PCE (%)	
n-i-p junction							
#1	Mesoscopic	CuSCN	FTO/cp-TiO$_2$/mp-TiO$_2$/PsK/CuSCN/Au	630	14.5	4.9	[10]
#2	Mesoscopic	CuSCN	FTO/cp-TiO$_2$/mp-TiO$_2$/Sb$_2$S$_3$/PsK/CuSCN/Au	570	17.2	5.12	[12]
#3	Mesoscopic	CuSCN	FTO/cp-TiO$_2$/mp-TiO$_2$/PsK/CuSCN/Au	1016	19.7	12.4	[9]
#4	Mesoscopic	CuI	FTO/cp-TiO$_2$/mp-TiO$_2$/PsK/CuI/Au	550	17.8	6	[13]
#5	Mesoscopic	NiO	FTO/cp-TiO$_2$/ mp-TiO$_2$PsK/mp-NiO/carbon	890	18.2	11.4	[38]
p-i-n junction							
#6	Planar	CuSCN	FTO/CuSCN/PsK/PCBM/Ag	677	8.8	3.8	[11]
#7	Planar	NiO	FTO/NiO/PsK/PCBM/Ag	786	14.2	7.3	[11]
#8	Planar	NiO	ITO/NiO$_x$ (solution)/PsK/PCBM/BCP/Al	920	12.4	7.8	[15]
#9	Planar	NiO	ITO/NiO/PsK/PCBM/Al	1050	15.4	7.6	[14]
#10	Planar	NiO	FTO/ NiO(sputter)/PsK/PCBM/BCP/Au	1100	15.2	9.8	[19]
#11	Planar	NiO	ITO/Cu:NiO$_x$/PsK/PC$_{61}$BM/C$_{60}$/Ag	1110	19.0	15.4	[20]
#12	Mesocopic	NiO	FTO/cp-NiO/mp- NiO/PsK/PCBM/Al	830	4.9	1.5	[18]
#13	Mesocopic	NiO	FTO/NiO(sol-gel)/PsK/PCBM/Au	882	16.3	9.1	[21]
#14	Mesoscopic	NiO	ITO/NiO$_x$(solution)/mp-NiO/PsK/PCBM/BCP/Al	1040	13.2	9.5	[17]
#15	Mesoscopic	NiO	ITO/NiO$_x$(sputter)/mp-NiO/PsK/PCBM/BCP/Al	960	19.8	11.6	[16]
#16	Super-mesoscopic	NiO	ITO/NiO$_x$(spray)/mp-Al$_2$O$_3$/PsK/PCBM/BCP/Ag	1040	18.0	13.5	[22]

Notes and References

[a] Department of Photonics, National Cheng Kung University, Tainan, Taiwan 701.

[b] Research Center for Energy Technology and Strategy (RCETS), National Cheng Kung University, Tainan, Taiwan 701.

[c] Advanced Optoelectronic Technology Center (AOTC), National Cheng Kung University, Tainan, Taiwan 701.

*E-mail: petercyc@mail.ncku.edu.tw

1. H.-S. Kim, C.-R. Lee, J.-H. Im, K.-B. Lee, T. Moehl, A. Marchioro, S.-J. Moon, R. Humphry-Baker, J.-H. Yum, J. E. Moser, M. Grätzel and N.-G. Park, *Sci. Rep.*, 2012, 2, 1-7.
2. K. Tanaka, T. Takahashi, T. Ban, T. Kondo, K. Uchida and N. Miura, *Solid state commun.*, 2003, 127, 619-623.
3. G. Xing, N. Mathews, S. Sun, S. S. Lim, Y. M. Lam, M. Grätzel, S. Mhaisalkar and T. C. Sum, *Science*, 2013, 342, 344-347.
4. S. D. Stranks, G. E. Eperon, G. Grancini, C. Menelaou, M. J. P. Alcocer, T. Leijtens, L. M. Herz, A. Petrozza and H. J. Snaith, *Science*, 2013, 342, 341-344.
5. A. Kojima, K. Teshima, Y. Shirai and T. Miyasaka, *J. Am. Chem. Soc.*, 2009, 131, 6050-6051.
6. J.-H. Im, C.-R. Lee, J.-W. Lee, S.-W. Park and N.-G. Park, *Nanoscale*, 2011, 3, 4088-4093.
7. M. M. Lee, J. Teuscher, T. Miyasaka, T. N. Murakami and H. J. Snaith, *Science*, 2012, 338, 643-647.
8. H. Zhou, Q. Chen, G. Li, S. Luo, T.-B. Song, H.-S. Duan, Z. Hong, J. You, Y. Liu and Y. Yang, *Science*, 2014, 345, 542-546.
9. P. Qin, S. Tanaka, S. Ito, N. Tetreault, K. Manabe, H. Nishino, M. K. Nazeeruddin and M. Grätzel, *Nat. Commun.* , 2014, 5, 1-6.
10. S. Ito, S. Tanaka, H. Vahlman, H. Nishino, K. Manabe and P. Lund, *ChemPhysChem*, 2014, 15, 1194-1200.
11. A. S. Subbiah, A. Halder, S. Ghosh, N. Mahuli, G. Hodes and S. K. Sarkar, *J. Phys. Chem. Lett.* , 2014, 5, 1748-1753.
12. S. Ito, S. Tanaka, K. Manabe and H. Nishino, *J. Phys. Chem. C*, 2014, 118, 16995-17000.
13. J. A. Christians, R. C. M. Fung and P. V. Kamat, *J. Am. Chem. Soc.*, 2014, 136, 758-764.
14. L. Hu, J. Peng, W. Wang, Z. Xia, J. Yuan, J. Lu, X. Huang, W. Ma, H. Song, W. Chen, Y.-B. Cheng and J. Tang, *ACS Photonics*, 2014, 1, 547-553.
15. J.-Y. Jeng, K.-C. Chen, T.-Y. Chiang, P.-Y. Lin, T.-D. Tsai, Y.-C. Chang, T.-F. Guo, P. Chen, T.-C. Wen and Y.-J. Hsu, *Adv. Mater.*, 2014, 26, 4107-4113.
16. K.-C. Wang, P.-S. Shen, M.-H. Li, S. Chen, M.-W. Lin, P. Chen and T.-F. Guo, *ACS Appl. Mater. Interfaces*, 2014, 6, 11851-11858.

17. K.-C. Wang, J.-Y. Jeng, P.-S. Shen, Y.-C. Chang, E. W.-G. Diau, C.-H. Tsai, T.-Y. Chao, H.-C. Hsu, P.-Y. Lin, P. Chen, T.-F. Guo and T.-C. Wen, *Sci. Rep.*, 2014, 4, 1-8.

18. H. Tian, B. Xu, H. Chen, E. M. J. Johansson and G. Boschloo, *ChemSusChem*, 2014, 7, 2150-2153.

19. J. Cui, F. Meng, H. Zhang, K. Cao, H. Yuan, Y. Cheng, F. Huang and M. Wang, *ACS Appl. Mater. Interfaces*, 2014, DOI: 10.1021/am507108u.

20. J. H. Kim, P.-W. Liang, S. T. Williams, N. Cho, C.-C. Chueh, M. S. Glaz, D. S. Ginger and A. K.-Y. Jen, *Adv. Mater.* , 2014, DOI: 10.1002/adma.201404189.

21. Z. Zhu, Y. Bai, T. Zhang, Z. Liu, X. Long, Z. Wei, Z. Wang, L. Zhang, J. Wang, F. Yan and S. Yang, *Angew. Chem.*, 2014, 126, 1-6.

22. W. Chen, Y. Wu, J. Liu, C. Qin, X. Yang, A. Islam, Y.-B. Cheng and L. Han, *Energy Environ. Sci.*, 2014, DOI: 10.1039/C4EE02833C.

23. J.-H. Im, I.-H. Jang, N. Pellet, M. Grätzel and N.-G. Park, *Nat. Nanotechnol.*, 2014, 9, 927-932.

24. M. Xiao, F. Huang, W. Huang, Y. Dkhissi, Y. Zhu, J. Etheridge, A. Gray-Weale, U. Bach, Y.-B. Cheng and L. Spiccia, *Angew. Chem. Int. Ed.*, 2014, 53, 1-7.

25. N. J. Jeon, J. H. Noh, Y. C. Kim, W. S. Yang, S. Ryu and S. I. Seok, *Nat. Mater.* , 2014, 13, 897-903.

26. M. Liu, M. B. Johnston and H. J. Snaith, *Nature* 2013, 501, 395-398.

27. Q. Chen, H. Zhou, Z. Hong, S. Luo, H.-S. Duan, H.-H. Wang, Y. Liu, G. Li and Y. Yang, *J. Am. Chem. Soc.*, 2014, 136, 622-625.

28. J. Seo, S. Park, Y. C. Kim, N. J. Jeon, J. H. Noh, S. C. Yoon and S. I. Seok, *Energy Environ. Sci.*, 2014, 7, 2642-2646.

29. M. D. Irwin, D. B. Buchholz, A. W. Hains, R. P. H. Chang and T. J. Marks, *PNAS*, 2008, 105, 2783–2787.

30. J. R. Manders, S.-W. Tsang, M. J. Hartel, T.-H. Lai, S. Chen, C. M. Amb, J. R. Reynolds and F. So, *Adv. Funct. Mater.*, 2013, 23, 2993-3001.

31. H.-Q. Wang, N. Li, N. S. Guldal and C. J. Brabec, *Org. Electron.*, 2012, 13, 3014-3021.

32. Y. Sun, C. J. Takacs, S. R. Cowan, J. H. Seo, X. Gong, A. Roy and A. J. Heeger, *Adv. Mater.*, 2011, 23, 2226-2230.

33. Y.-J. Lee, J. Yi, G. F. Gao, H. Koerner, K. Park, J. Wang, K. Luo, R. A. Vaia and J. W. P. Hsu, *Adv. Energy Mater.*, 2012, 2, 1193-1197.

34. B. O'Regan, F. Lenzmann, R. Muis and J. Wienke, *Chem. Mater.*, 2002, 14, 5023-5029.

35. J. A. Christians and P. V. Kamat, *ACS Nano* 2013, 7, 7967-7974.

36. M. Rusop, T. Soga, T. Jimbo and M. Umeno, *Surf. Rev. Lett.*, 2004, 11, 577-583.

37. K. Tennakone, G. R. R. A. Kumara, A. R. Kumarasinghe, K. G. U. Wijayantha and P. M. Sirimanne, *Semicond. Sci. Tech.*, 1995, 10, 1689-1693.

38. Z. Liu, M. Zhang, X. Xu, L. Bu, W. Zhang, W. Li, Z. Zhao, M. Wang, Y.-B. Cheng and H. He, *Dalton Trans.*, 2014, DOI: 10.1039/C4DT02904F.

39. J. He, H. Lindström, A. Hagfeldt and S.-E. Lindquist, *J. Phys. Chem. B*, 1999, 103, 8940-8943.

40. S. Powar, T. Daeneke, M. T. Ma, D. Fu, N. W. Duffy, G. Götz, M. Weidelener, A. Mishra, P. Bäuerle, L. Spiccia and U. Bach, *Angew. Chem. Int. Ed.*, 2013, 52, 602-605.

41. F. Odobel and Y. Pellegrin, *J. Phys. Chem. Lett.*, 2013, 4, 2551-2564.

42. P. Docampo, J. M. Ball, M. Darwich, G. E. Eperon and H. J. Snaith, *Nat. Commun.*, 2013, 4, 1-6.

43. H.-Y. Hsu, C.-Y. Wang, A. Fathi, J.-W. Shiu, C.-C. Chung, P.-S. Shen, T.-F. Guo, P. Chen, Y.-P. Lee and E. W.-G. Diau, *Angew. Chem.*, 2014, 126, 9493-9496.

44. L. Etgar, P. Gao, Z. Xue, Q. Peng, A. K. Chandiran, B. Liu, Md K. Nazeeruddin and M. Grätzel, *J. Am. Chem. Soc.*, 2012, 134, 17396-17399.

45. W. A. Laban and L. Etgar, *Energy Environ. Sci.*, 2013, 6, 3249-3253.

46. J. Shi, J. Dong, S. Lv, Y. Xu, L. Zhu, J. Xiao, X. Xu, H. Wu, D. Li, Y. Luo and Q. Meng, *Appl. Phys. Lett.*, 2014, 104, -.

47. Y. Xiao, G. Han, Y. Li, M. Li, Y. Chang and J. Wu, *J. Mater. Chem. A*, 2014, 2, 16531-16537.

48. Y. Xiao, G. Han, Y. Li, M. Li and J. Wu, *J. Mater. Chem. A*, 2014, 2, 16856-16862.

49. H. Hu, D. Wang, Y. Zhou, J. Zhang, S. Lv, S. Pang, X. Chen, Z. Liu, N. P. Padture and G. Cui, *RSC Advances*, 2014, 4, 28964-28967.

50. Z. Ku, Y. Rong, M. Xu, T. Liu and H. Han, *Sci. Rep.*, 2013, 3.

51. A. Mei, X. Li, L. Liu, Z. Ku, T. Liu, Y. Rong, M. Xu, M. Hu, J. Chen, Y. Yang, M. Grätzel and H. Han, *Science*, 2014, 345, 295-298.

52. M. Xu, Y. Rong, Z. Ku, A. Mei, T. Liu, L. Zhang, X. Li and H. Han, *J. Mater. Chem. A*, 2014, 2, 8607-8611.

53. Y. Rong, Z. Ku, A. Mei, T. Liu, M. Xu, S. Ko, X. Li and H. Han, *J. Phys. Chem. Lett.*, 2014, 5, 2160-2164.

54. Z. Li, S. A. Kulkarni, P. P. Boix, E. Shi, A. Cao, K. Fu, S. K. Batabyal, J. Zhang, Q. Xiong, L. H. Wong, N. Mathews and S. G. Mhaisalkar, *ACS Nano*, 2014, 8, 6797-6804.